Supporting information

Integration of Fe_xS Electrocatalysts and Simultaneously Generated Interfacial Oxygen Vacancies to Synergistically Boost Photoelectrochemical Water Splitting of Fe_2O_3 Photoanodes

Aizhen Liao,[a, 1] Ruotian Chen,[d, e, 1] Fengtao Fan,[d, e, *] Leixin Xiao,[f] Huichao He,[c] Chunfeng Zhang,[a] Adullah M. Asiri,[b] Yong Zhou,[a, g, *] Can Li,[d, e] and Zhigang Zou[a, f, g]

[a]*National Laboratory of Solid State Microstructures, Collaborative Innovation Center of Advanced Microstructures, School of Physics, Nanjing University, Nanjing 210093, P. R. China.*

[b]*Center of Excellence for Advanced Materials Research, Chemistry of Department, Faculty of Science, King Abdulaziz University, Jeddah 21589, Saudi Aribia.*

[c] *State Key Laboratory of Environmental Friendly Energy Materials, School of Materials Science and Engineering, Southwest University of Science and Technology, Mianyang, Sichuan 621010, P. R. China.*

[d]*State Key Laboratory of Catalysis, Dalian National Laboratory for Clean Energy, The Collaborative Innovation Centre of Chemistry for Energy Materials (iChEM), Dalian Institute of Chemical Physics, Chinese Academy of Sciences, Dalian 116023, P. R. China.*

[e]*University of Chinese Academy of Sciences, Beijing 100049, P. R. China.*

[f] *School of Engineering and Applied Science, Nanjing University, Nanjing 210093, P. R. China.*

[g]*Sunlite Ltc, Kunshan Innovation Institute of Nanjing University Kunshan, Jiangsu 215347, P. R. China.*

[1] *Liao and Chen equally contribute to the work*

Experimental section

Synthesis of $Fe_2O_3|V_o|Fe_xS$ photoanode: Firstly, FeOOH nanorods were vertically aligned on the FTO substrate according to reported methods by our group.[21] More details had been described previously. FeOOH and sulfur powder separately were placed at two heating zones of a pipe furnace. With increase of temperature of the furnace to 300 °C under argon atmosphere, sulfur powder sublimed into the gas phase (sulfur sublimation temperature of ~ 95 °C) and reacted with the surface of the FeOOH nanorod arrays for 30 min to generate a thin layer of Fe_xS. To grow the Fe_xS, the FeOOH nanorod arrays were placed 15 cm apart from the S powder (sulfur, AR, 99.9%), inside a quartz tube. With ~199 sccm of high-purity Ar gas as the carrier gas, the furnace temperature was raised to 300 °C. After 30 min of sulfuration, the furnace was allowed to cool to room temperature under the argon flow, followed by heating at 550 °C for 120 minutes in Ar gas, and subsequently at 650 °C for 15 min to result in the coating of Fe_xS on the Fe_2O_3 nanorod. As comparison, the pristine Fe_2O_3 nanorods were also synthesized under the same growth conditions without the sulfuration process.

Sample characterizations: A FEI NOVA NanoSEM230 scanning electron microscope was employed to investigate the morphology of samples. The crystal structure of samples was identified by X-ray diffraction (XRD) (Ultima III, Rigaku) with Cu Ka radiation (k = 0.154 nm). Transmission electron microscope (TEM) images were taken on a JEM 200CX TEM apparatus. X-ray photoelectron spectroscopy (XPS) was carried out on a Thermo Scientific K-Alpha instrument operating with an unmonochromatized Al Ka X-ray source, and the data were calibrated by the binding energy of the C1s line at 283.6 eV. A Shimadzu UV-2550 spectrometer equip with an integrating sphere was used to investigate the absorption properties of samples. Electrochemical impedance spectroscopic (EIS) curves were measured by a PAR2273 workstation (CHI-633E, Shanghai Chenhua) under a forward bias of 0.2 V and AM 1.5G illumination. The frequency ranged from 0.1 mHz to 100 kHz. The Mott-Schottky curves were measured in 1 M NaOH aqueous solution using an electrochemical analyzer (Princeton Applied Research, 2273). The surface photovoltage microscopy (SPVM) and conductive atomic force microscopy (C-AFM) measurements were performed by a commercial AFM

system (Bruker Dimension Icon) equipped with a 450-nm laser to excite the sample. The Bruker SCM-PIT probe was used for both SPVM and C-AFM mapping. For the SPVM mapping, the AM-KPFM mode was used and the SPVM images were obtained by direct subtraction between a steady-state illuminated and a dark KPFM scan at the same location. In the KPFM scan, the lift height of probe was set at 20 nm. For the C-AFM mapping, Peak Force TUNA mode was used. All scan parameters are optimized with respect to good signal-to-noise ratio.

Photoelectrochemical property measurements: The photoelectrochemical (PEC) performance of the photoanodes is investigated in a three-electrode cell using an electrochemical analyzer (CHI-630D, Shanghai Chenhua) under AM 1.5G illumination. The electrolyte is a 1 M NaOH aqueous solution (pH~13.6). The Fe_2O_3 sample is used as a working electrode. A Pt foil and a saturated Ag/AgCl electrode are used as a counter and a reference electrode. The RHE potential is calculated following the formula $V_{RHE} = V_{Ag/AgCl} + 0.059pH + E_{Ag/AgCl}$, where V_{RHE} is the converted potential versus RHE, and $E^{o}_{Ag/AgCl} = 0.1976$ V at 25 ^{o}C. The active area of the Fe_2O_3 sample is fixed to 0.28 cm^2 using a black mask. A cyclic voltammetry method is adopted with a scan rate of 10 mV s^{-1}.

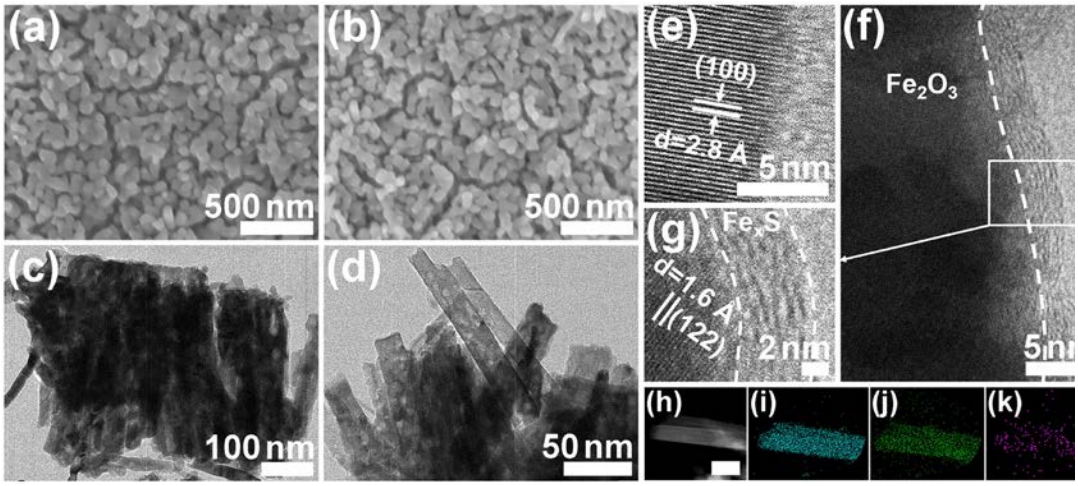

Fig. S1 (a, b) SEM images and (c, d) TEM images of Fe_2O_3 and $Fe_2O_3|V_o|Fe_xS$, respectively. (e) HRTEM images for Fe_2O_3. (f) HRTEM images of $Fe_2O_3|V_o|Fe_xS$, (g) enlarged image of (f). (h-k) for the TEM and the corresponding EDS mapping images of O, Fe and S for $Fe_2O_3|V_o|Fe_xS$, respectively, the scale bar is 500 nm.

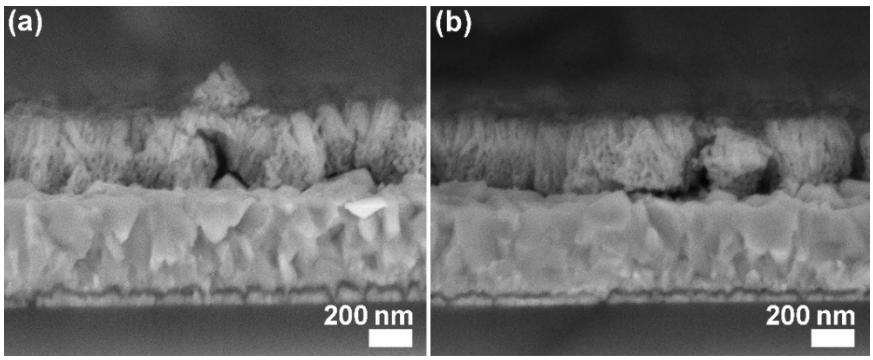

FIG. S2 (a) and (b) The cross-sectional views of Fe_2O_3 and $Fe_2O_3|V_o|Fe_xS$, respectively.

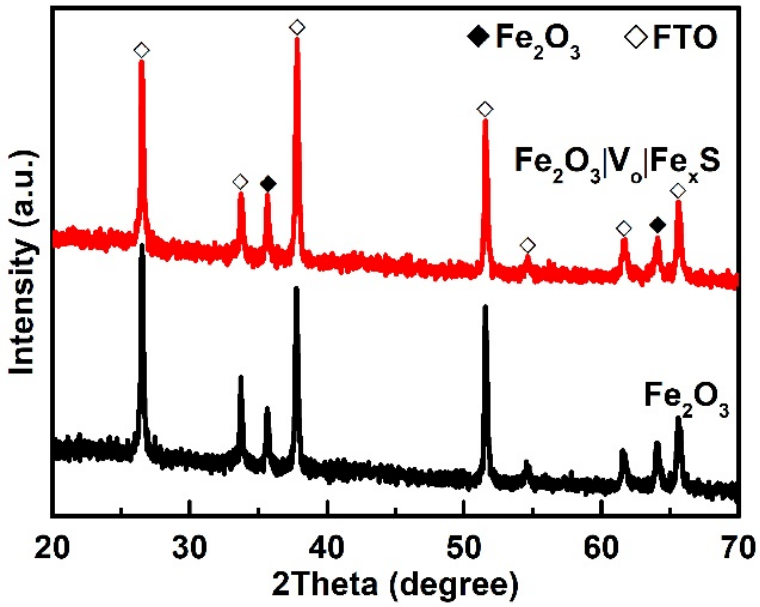

Fig. S3 XRD patterns of Fe_2O_3 and $Fe_2O_3|V_o|Fe_xS$.

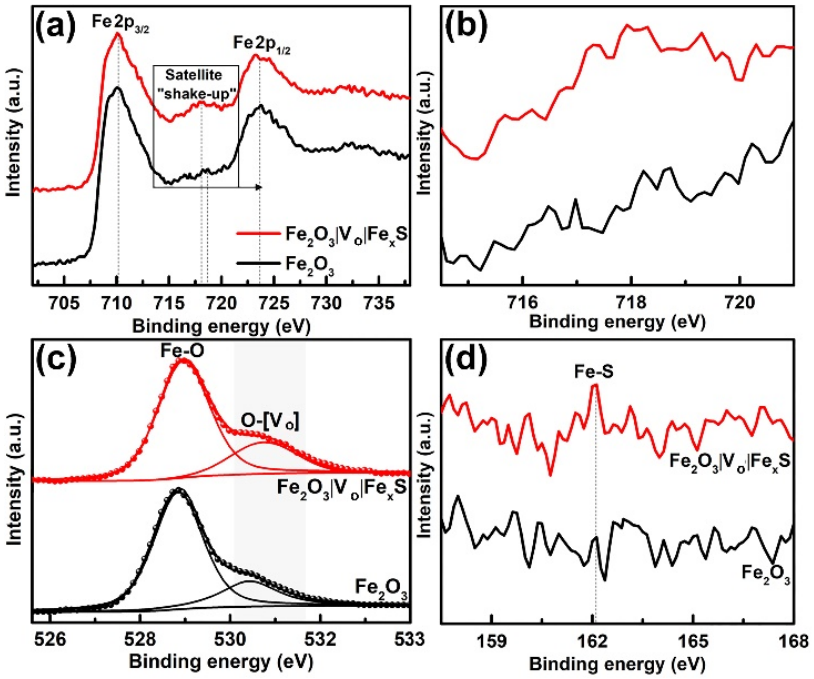

Fig. S4 XPS high resolution (a) Fe 2p, (b) enlarged image of (a), the Fe^{2+} signal peak is labelled with black circles. (c) O 1s, and (d) S 2p spectra of Fe_2O_3 and $Fe_2O_3|V_o|Fe_xS$.

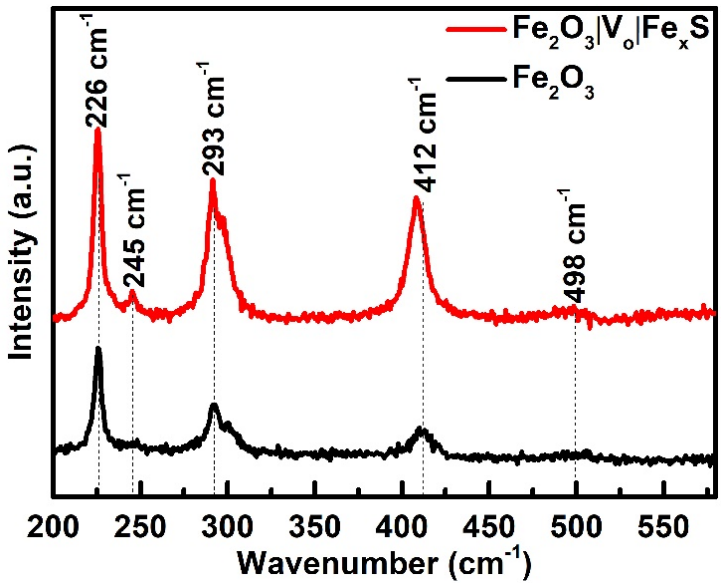

Fig. S5 Raman spectra of Fe_2O_3 and $Fe_2O_3|V_o|Fe_xS$.

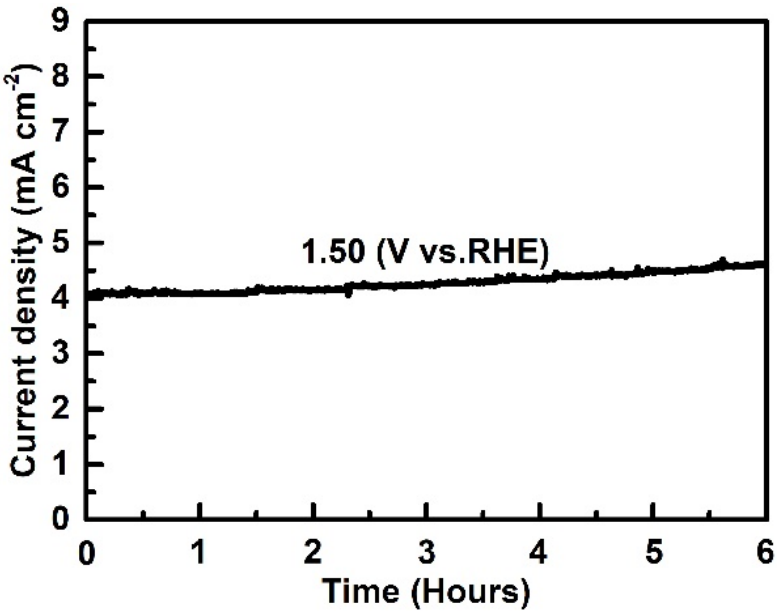

Fig. S6 Current density versus time measured at the potential of 1.50 V vs. RHE for a typical $Fe_2O_3|V_o|Fe_xS$.

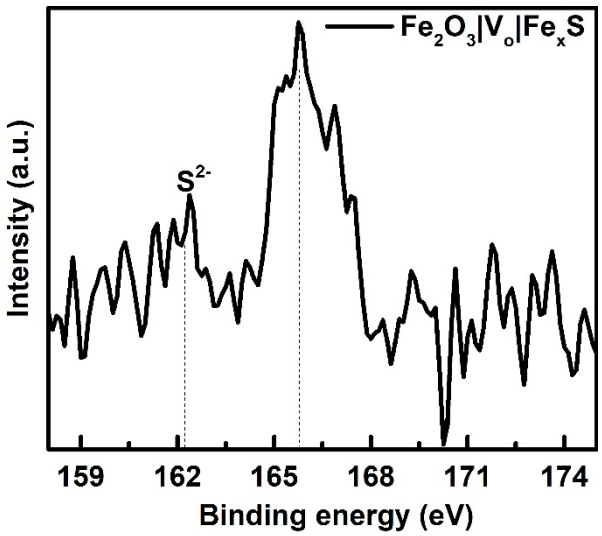

Fig. S7 XPS high resolution S 2p spectra of $Fe_2O_3|V_o|Fe_xS$ after the stability test.

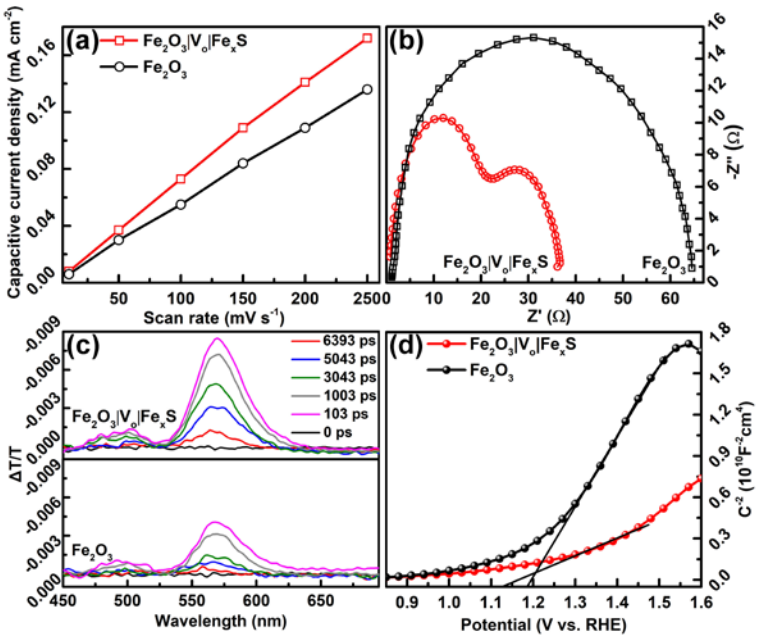

Fig. S8 (a) Plot of scan rate against the difference in the double layer charging current at 1.23 V vs. RHE, (b) EIS spectra, (c) Transient absorption spectra excited by UV laser pulses (350 nm), and (d) Mott-Schottky plots collected at 1 kHz in the dark of Fe_2O_3 an $Fe_2O_3|V_o|Fe_xS$, respectively.

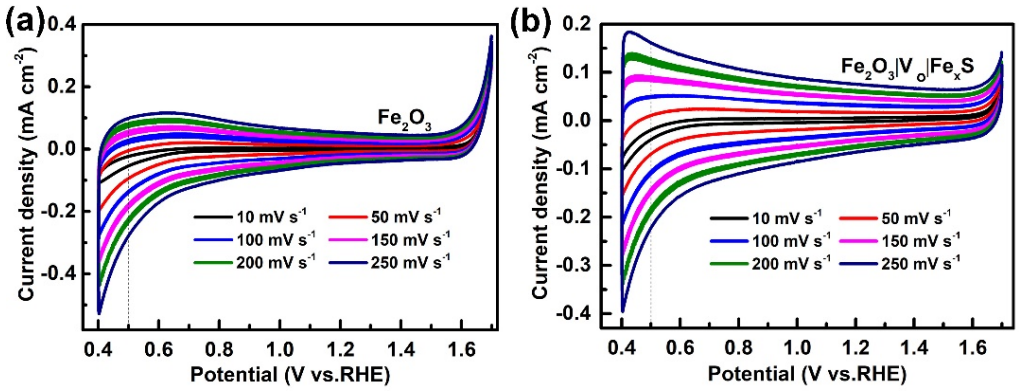

Fig. S9 (a) and (b) Cyclic voltammograms curves of Fe_2O_3 and $Fe_2O_3|V_o|Fe_xS$ at the scan rate from 10 to 250 mV s^{-1}.

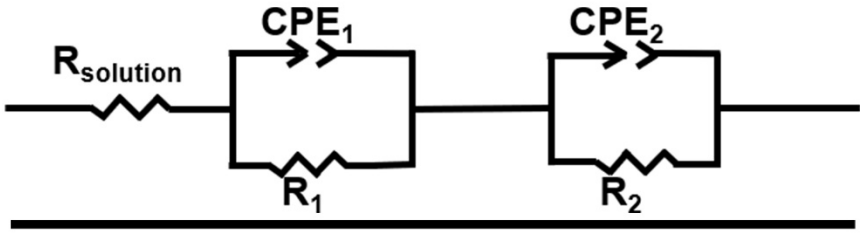

(R/Ω cm^2)	$R_{solution}$	R_1	R_2
Fe_2O_3	1.431	35.21	70.59
Fe_2O_3|V_o|Fe_xS	1.321	30.21	22.12

Fig. S10 The equivalent circuit model for data fitting of Figure S8b, as well as the fitting results.

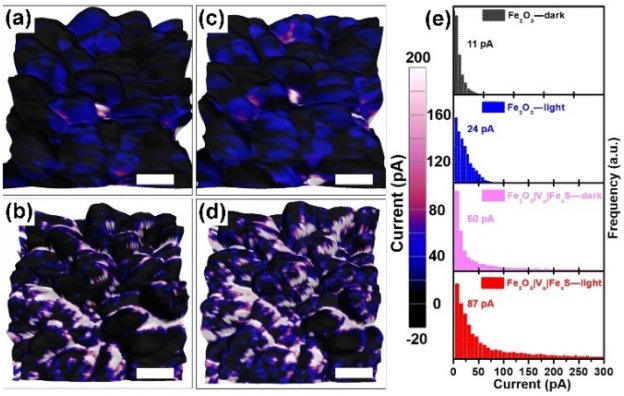

Fig. S11 (a-d) Current images of Fe_2O_3 (a, c) and $Fe_2O_3|V_o|Fe_xS$ (b, d) electrodes collected under dark (a, b) and under illumination (c, d) conditions, mapped by C-AFM at a +1 V sample bias. Scale bars in a-d, 200 nm. The current bar (from -20 pA to 200 pA) is applicable to a-d. (e) Histograms of the current distributions on Fe_2O_3 and $Fe_2O_3|V_o|Fe_xS$ electrodes under dark and illumination conditions and at a +1 V sample bias. The means of the current (11, 24, 60 and 87 pA) are marked in the figure. The illumination condition is created by the 450-nm laser with light intensity of 4 mV/cm^2.

Table S1. Comparison of previously reported photocurrent density of Fe_2O_3 electrode with our result at 1.5 V vs. RHE

Composite	J_{photo} at 1.5 V (mA/cm^2)	Electrolyte	Scan rate (mV/s)	Synthesis methods	Ref.
$FeOOH/Fe_2O_3$	1.6	1 M NaOH	10	Precipitation method	(1)
$C/Co_3O_4/Fe_2O_3$	2.0	1 M NaOH	—	Hydrothermal approach	(2)
Co_3O_4/Fe_2O_3	1.75	1 M NaOH	—	In situ hydrothermal	(3)
$Co(OH)_2/Co_3O_4/Fe_2O_3$	2.0	0.1 M KOH	20	ALD	(4)
$Ni(OH)_2/IrO_2/Fe_2O_3$	2.0	1 M NaOH	—	Successive ion layer adsorption (SILA) method	(5)
$NiOOH/Fe_2O_3$	2.1	1 M NaOH	20	Photoassisted electrodeposition	(6)
$FeOOH/Fe_2O_3$	1.6	1 M NaOH	—	Solution-based precipitation	(7)
$Ni(OH)_2/Fe_2O_3$	0.55	1 M NaOH	20	Hydrothermal method	(8)
$NiFeO_x/Al_2O_3/Fe_2O_3$	3.3	1 M NaOH	10	Photoelectrochemical	(9)
$NiBi/Fe_2O_3$	0.9	1 M KOH	50	Photochemical deposition	(10)
$Ni(OH)_2/Fe_2O_3$	2.0	1 M NaOH	50	Dipping method	(11)
$NiFeO_x/Fe_2O_3$	0.67	1 M NaOH	—	Drop-casting	(12)
NiO_x/Fe_2O_3	0.8	1 M NaOH	10	Photodeposited	(13)
$Ti\text{-}FeOOH/Fe_2O_3$	4.10	1 M NaOH	20	Hydrothermal deposition	(14)
$Fe_2O_3\|Vo\|Fe_xS$	4.25	1 M NaOH	10	CVD	**This work**
Co_3O_4/Fe_2O_3	0.66	1 M NaOH	10	Plasma-assisted route	(15)

References

1 J. Y. Kim, D. H. Youn, K. Kang and J. S. Lee, *Angew. Chem. Int. Ed.*, 2016, **55**, 10854-10858.

2 P. Zhang, T. Wang, X. X. Chang, L. Zhang and J. L. Gong, *Angew. Chem. Int. Ed.*, 2016, **55**, 5851-5855.

3 L. Xi, P. D. Tran, S. Y. Chiam, P. S. Bassi, W. F. Mak, H. K. Mulmudi, S. K. Batabyal, J. Barber, J. S. C. Loo, L. H. Wong, *J. Phys. Chem. C*, 2012, **116**, 13884-13889.

4 S. C. Riha, B. M. Klahr, E. C. Tyo, S. N. Seifert, S. Vajda, M. J. Pellin, T. W. Hamann, A. B.

Martinson, *ACS nano*, 2013, **7**, 2396-2405.

5 Z. Wang, G. Liu, C. Ding, Z. Chen, F. Zhang, J. Shi, C. Li, *J. Phys. Chem. C*, 2015, **119**, 19607-19612.

6 A. G. Tamirat, W. -N. Su, A. A. Dubale, H. -M. Chen, B. -J. Hwang, *J. Mater. Chem. A*, 2015, **3**, 5949-5961.

7 J. Y. Kim, D. H. Youn, K. Kang, J. S. Lee, *Angew. Chem. Int. Ed.*, 2016, **55**, 10854-10858.

8 Q. Li, J. Bian, N. Zhang and D. H. Ng, *Electrochimica Acta*, 2015, **155**, 383-390.

9 C. G. Morales-Guio, M. T. Mayer, A. Yella, S. D. Tilley, M. Grätzel, X. Hu, *J. Am. Chem. Soc.*, 2015, **137**, 9927-9936.

10 Y.-R. Hong, Z. Liu, S. F. B. Al-Bukhari, C. J. J. Lee, D. L. Yung, D. Chi, T. A. Hor, *Chem. Commun.*, 2011, **47**, 10653-10655.

11 G. Wang, Y. Ling, X. Lu, T. Zhai, F. Qian, Y. Tong and Y. Li, *Nanoscale*, 2013, **5**, 4129-4133.

12 C. Du, X. Yang, M. T. Mayer, H. Hoyt, J. Xie, G. McMahon, G. Bischoping, D. Wang, *Angew. Chem. Int. Ed.*, 2013, **52**, 12692-12695.

13 F. Malara, F. Fabbri, M. Marelli, A. Naldoni, *ACS Catal.*, 2016, **6**, 3619-3628.

14 K. -Y. Yoon, H. -J. Ahn, M. -J. Kwak, S. -I. Kim, J. Park, J. -H. Jang, *J. Mater. Chem. A*, 2016, **4**, 18730-18736.

15 G. Carraro, C. Maccato, A. Gasparotto, K. Kaunisto, C. Sada, D. Barreca, *Plasma Process. Polym.*, 2016, **13**, 191-200.